Switchable Underwater Adhesion by Deformable Cupped Microstructures

Yue Wang, Victor Kang, Walter Federle, Eduard Arzt, and René Hensel*

Switchable underwater adhesion can be useful for numerous applications, but is extremely challenging due to the presence of water at the contact interface. Here, deformable cupped microstructures (diameter typically 100 μm, rim thickness 5 μm) are reported that can switch between high (≈1 MPa) and low (<0.2 MPa) adhesion strength by adjusting the retraction velocity from 100 to 0.1 μm s^{-1}. The velocity at which the switch occurs is determined by specific design parameters of the cupped microstructure, such as the cup width and angle. The results are compared with theoretical estimates of water penetration into the contact zone and expansion of the cup during retraction. This work paves the way for controlling wet adhesion on demand and may inspire further applications in smart adhesives.

1. Introduction

Robust wet adhesion with the ability to release on demand remains a challenge despite numerous potential applications in a variety of areas such as underwater soft robotics,[1,2] transportation,[3,4] biomedicine,[5,6] and tissue engineering.[7,8] Nonpermanent, reversible adhesives often rely on van der Waals interactions,[9,10] capillary forces,[11,12] or dynamic bonds.[13] In completely immersed contacts, capillary forces no longer contribute to adhesion. Furthermore, van der Waals interactions are drastically reduced when liquids are present in the contact.[14,15] The stability of liquid in the contact zone depends mainly on the film's tendency to dewet, which is a function of the solid–solid and liquid–solid interfacial energies.[16,17] For example, water may be expelled from the contact if both surfaces are hydrophobic. On the other hand, if one of the surfaces is at least partially wettable, water remains in the contact.[18] Dynamic bonds

are an opportunity to improve adhesion in wet conditions.[13,19] However, these bonds inevitably require functional groups at the target surface and are subject to wear during repeated attachment–detachment cycles as in pick-and-place handling.

Microstructured elastomer surfaces are capable of reliable and switchable adhesion in dry environments.[20–23] Several groups have demonstrated their potential underwater, provided the water can be expelled from the contact region.[24,25] In particular, hydrophobic microstructures or microstructures with reentrant geometry have the ability to trap air in between the structures when immersed in water.[26–28] Such air bubbles can improve adhesion through the presence of capillary forces, even when the contact is fully immersed.[29,30] The microstructure tips can be further modified by introducing chemical bonds[3] or water absorbers such as hydrogels;[19] however, switchability by external stimuli remains elusive.

In nature, suction cups have evolved for temporary underwater adhesion during locomotion or when catching prey.[31,32] Many species, such as octopus,[31] clingfish,[32,33] and netwinged midge larvae[34] utilize muscular actuation to reduce the hydrostatic pressure in the contact and, therefore, to control the adhesive force. This principle has been translated to synthetic macroscopic grippers working in dry environments by adding pumps to control the air pressure. On the microscale, recent reports demonstrate the fabrication of microsucker arrays by micromachining or optical lithography combined with replica molding.[35–37] The reported adhesion to smooth silicon surfaces is in the range of 50–100 kPa in air and underwater. In a previous study,[38] we presented cupped microstructures (CMs) created by two-photon lithography and replica molding. Adhesion strengths of individual structures were about 1 MPa in air and underwater. Despite similar adhesive strengths in both media, adhesion mechanisms were attributed to suction under water and van der Waals interactions in dry conditions.

The present article explores the potential of deformable cupped microstructures, reminiscent of suction cups, for switchable adhesion in wet conditions. Underwater adhesion tests are systematically performed with constant retraction velocities ranging from 0.1 to 100 μm s^{-1} until detachment. Finally, we demonstrate underwater manipulation (pick-and-place) of a submerged object using an array of cupped microstructures.

Dr. Y. Wang, Prof. E. Arzt, Dr. R. Hensel
INM—Leibniz Institute for New Materials
Campus D2 2, Saarbrücken 66123, Germany
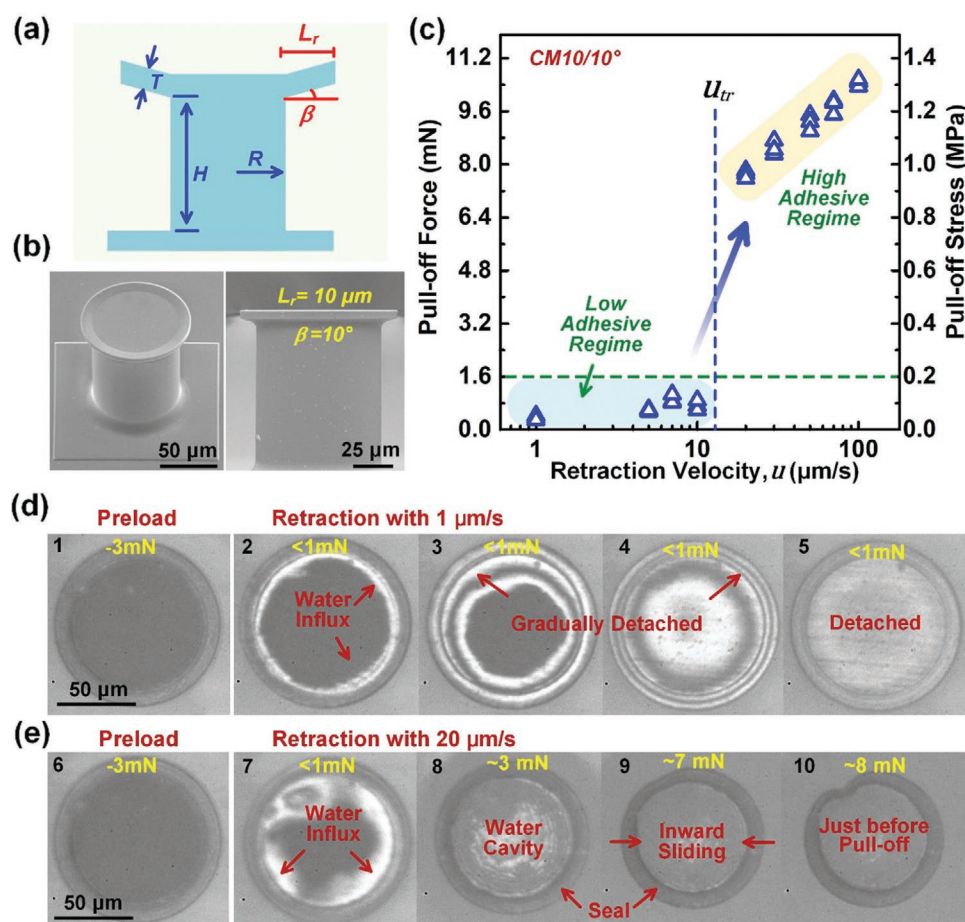E-mail: rene.hensel@leibniz-inm.de
Dr. V. Kang, Prof. W. Federle
Department of Zoology
University of Cambridge
Cambridge CB2 3EJ, UK
Prof. E. Arzt
Department of Materials Science and Engineering
Saarland University
Campus D2 2, Saarbrücken 66123, Germany

The ORCID identification number(s) for the author(s) of this article can be found under https://doi.org/10.1002/admi.202001269.

2. Results and Discussion

Cupped microstructures were generated by two-photon lithography using standard (meth)acrylate-based resin (**Figure 1**a).

Figure 1. Velocity-dependent adhesion of cupped microstructures. a) Schematic of a cupped microstructure, where H is the height and R is the radius of the stalk, T is the thickness, L_r is the projected width of the rim, and β is the cup angle. b) Scanning electron micrographs of the cupped microstructure CM10/10°. c) The underwater pull-off forces and stresses of single CM10/10° microstructures at different retraction velocities. d,e) Contact images for the two adhesion regimes. A dark rim indicates close contact and sealing; interference fringes indicate the beginning of detachment, whereas gray indicates thicker water layers. Note that the high pull-off forces in the adhesive regime are correlated with the appearance of strong seals.

Subsequently, these structures were used as templates for replication in polyurethane (PU) elastomers. The stalk height, H, and stalk radius, R, of each microstructure were 100 and 40 μm, respectively. The thickness of the rim, T, was 5 μm. We varied the projected width of the rim, L_r, and the cup angle, β. The adhesion of a first set of cupped microstructures with $L_r = 10 \; \mu m$ and $\beta = 10°$ (referred to as "CM10/10°," Figure 1b) to a nominally flat, smooth glass substrate was systematically tested underwater as a function of the retraction velocity varying from 0.1 to 100 μm s^{-1}. Pull-off stresses were calculated as the forces divided by the area of the undeformed cup (7854 μm^2). Figure 1c shows that pull-off forces, F_p, strongly depended on the retraction velocity. Adhesion was weak ($F_p < 1.6$ mN) for velocities up to 10 μm s^{-1}. For higher retraction velocities, the adhesion force drastically increased to values ranging between 7.8 and 10.8 mN. Thus, we obtained a velocity-dependent, sharp transition from a low adhesion regime to a high adhesion regime with pull-off forces increasing by one order of magnitude. In the adhesive regime, the pull-off force further increased with increasing velocities. Note that the resulting pull-off stresses were in excess of 1 MPa for high velocities.

This is far above the maximum adhesion strength expected from pure suction under dry conditions (≈ 0.1 MPa).

The in situ observations in Figure 1d,e show qualitative differences in the development of adhesive contacts in the two regimes. In both regimes, the contact was formed by compression of the cup during preloading (steps 1 and 6). During retraction, the behavior was different in the two adhesion regimes:

1. Low adhesion regime (low retraction velocity): Some initial water influx was visible from the white areas at the perimeter of the stalk (Figure 1d, step 2). The resulting detachment of the stalk was seen from the interference fringes visible in step 3 (Figure 1d). The detachment led to a cavity under the stalk that was further flooded with water during the pull-off. The expansion of the cavity is restricted by the influx through the outer rim, and by the incompressibility of water (Figure 1d, step 4). Finally, the whole structure detached (Figure 1d, step 5). In this regime, the pull-off force was below 1.6 mN (or 0.2 MPa), and the bright gray of the rim indicated that it was not in close surface contact (Figure 1d, steps 3–5).

2. High adhesion regime (high retraction velocity): The sequence of events (Figure 1e) differs here by the development of a larger and more stable seal at the perimeter (steps 6–9) before the final detachment of the structure (step 10). Consequently, the hydrostatic pressure in the cavity was reduced, causing the rim to be pressed more strongly against the substrate (visible by the dark gray of the rim, see Figure 1e, steps 8–10). As a result, water flow was further reduced, leading to an even lower cavity pressure and tighter seal. This self-sealing mechanism as described in our previous article[38] represents a positive feedback loop, which can explain the observed sharp increase of adhesion with pull-off velocity.

In summary, the retraction velocity and the resulting influx of water play a decisive role in the underwater adhesion of cupped microstructures.

To evaluate the impact of the cup design on the transition velocity, microstructures with projected width of the rim, L_r, of 10 and 20 µm and cup angles, β, of 0, 5, 10, and 15° were fabricated and tested. The results are shown in **Figure 2**. With increasing cup angles, the transition from the low-adhesive to the high-adhesive regime occurred at lower retraction velocities. For a cup with $L_r = 10$ µm, the transition occurred between 0.5 and 1 µm s^{-1} for a cup angle of 15°, whereas the transition was observed between 10 and 20 µm s^{-1} for cup angles of 5 and 10° (Figure 2a). A wider rim ($L_r = 20$ µm) further decreased the switching velocity. Hence, for microstructures with cup angles of 5 and 10°, the transition occurred between 2 and 3 µm s^{-1},
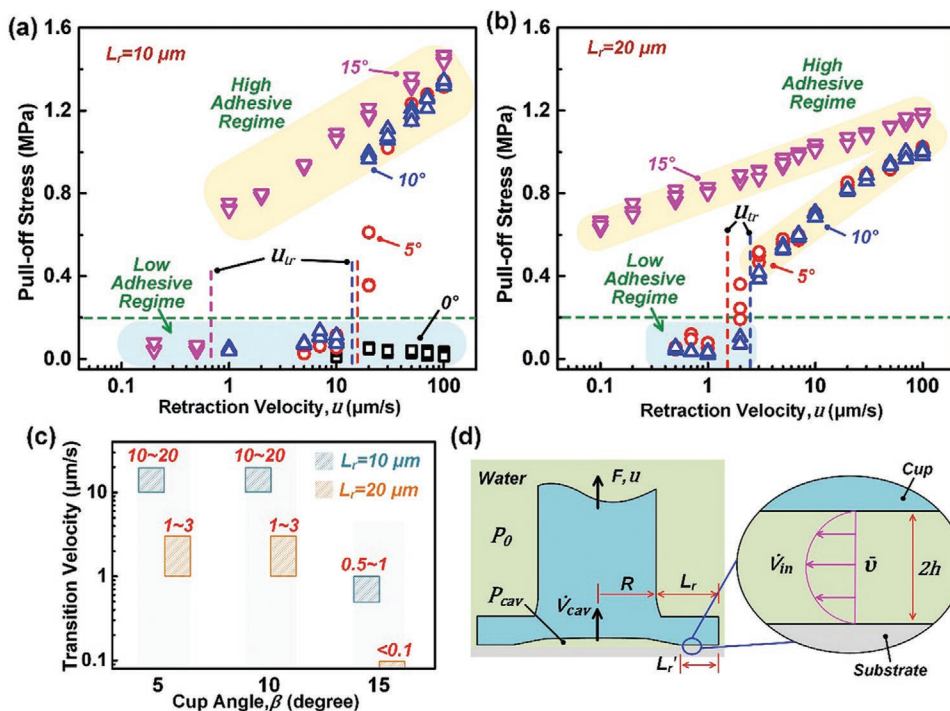
which is almost one order of magnitude lower compared to structures with $L_r = 10$ µm (Figure 2b). Interestingly, the cupped microstructure with $\beta = 15°$ was more adhesive than those with cup angles of 5 and 10° for all retraction velocities tested. It is important to note that, while the switching velocities varied depending on the cup angle and the rim width (summarized in Figure 2c), the maximum pull-off stresses were consistently high for all structures tested at 100 µm s^{-1}, ranging between 1.0 and 1.4 MPa.

To understand the transition from the low to the high adhesion regime, we developed a simple model for the detachment process as a function of the retraction velocity. A water-filled cavity develops under the cup before detachment, and its volume, $\dot{V}_{cav}$, expands over time (Figure 1d,e). However, this expansion is limited by the influx of water, $\dot{V}_{in}$, due to water incompressibility.

The water influx must approximately equal the volume expansion of the cavity, i.e.

$$\dot{V}_{in} \approx \dot{V}_{cav} \tag{1}$$

First, the stalk detaches from the substrate and forms the cavity. As this event always happened significantly before the peak pull-off force was reached, we assume that the distance between stalk and substrate surface is much larger than the distance between rim and surface, and that the pressure in the cavity is therefore uniform. The applied force will stretch the stalk $\Delta H \approx \dfrac{(p_0 - p_{cav}) H}{E}$, where H is the length and E is the

Figure 2. Dependence of pull-off stress on retraction velocity for different widths of the rim and cup angles. Projected width of the rim of a) 10 µm and b) 20 µm. The vertical dashed lines highlight the transition velocity, u_{tr}. Cup angles were 0°, 5°, 10°, and 15°. Each test was repeated three times with the same microstructure. c) Transition velocity as a function of the design parameters. Note that the transition to higher adhesion is shifted to lower velocities for wider rims, L_r, and larger cup angles, β. d) Schematic defining the dimensions R and L_r for the cup and the pressure, p_{cav}, and volume growth rate, $\dot{V}_{cav}$, for the cavity. The insert shows the geometry and laminar flow pattern assumed allowing influx of water, at a rate $\dot{V}_{in}$, into the cavity. The width of the seal is L_r'. The thickness of the liquid film in the seal between rim and substrate is denoted as $2h$.

**ADVANCED
SCIENCE NEWS**

www.advancedsciencenews.com

**ADVANCED
MATERIALS
INTERFACES**

www.advmatinterfaces.de

Young's modulus of the stalk, and $p_0 - p_{cav}$ is the pressure difference between hydrostatic pressure outside the contact, p_0, and inside the cavity, p_{cav}. Therefore, the cavity expands vertically at a rate

$$\dot{V}_{cav} \approx \pi R^2 \left(u - \frac{d\Delta H}{dt} \right) = \pi R^2 \left(u - \frac{H}{E} \frac{d(p_0 - p_{cav})}{dt} \right) \quad (2)$$

where πR^2 is the area of the stalk and u is the retraction velocity (Figure 2d).

It is assumed that, in the seal, a homogeneously thin water film separates the cup and the substrate due to the hydrophilic glass substrate. Thus, the water influx is given by

$$\dot{V}_{in} = 4\pi\, Rh\overline{v} \quad (3)$$

where $2\pi R$ is the perimeter of the stalk, $2h$ is the thickness of the water film between the seal and the substrate, and $\overline{v}$ is the average flow velocity, which for laminar flow is $\frac{h^2(p_0 - p_{cav})}{3\mu L_r'}$, where μ is the viscosity of water, and L_r' is the width (=radial length) of the seal (Figure 2d).

Rewriting Equation (1) gives a pull-off stress (based on suction)

$$\sigma_p = p_0 - p_{cav} = \frac{3\mu\, RL_r'}{4h^3} u_{eff} \quad (4)$$

where $u_{eff} = u\left(1 - e^{-\frac{4h^3 E}{3\mu L_r' RH} t}\right)$ is the effective retraction velocity (for details, see Supporting Information).

A faster pull will lead to higher adhesion strength. Equation (4) predicts that assuming an unchanged seal (L_r', h), the pressure difference and thereby adhesion strength should increase linearly with retraction velocity. However, the data shown in Figures 1 and 2 show that the adhesion is low for small velocities, and then exhibits a sudden, stepwise increase, followed by a logarithmic increase for higher velocities. How can this stepwise increase of adhesion be explained? The larger pressure difference caused by a faster pull will press the rim of the cup more firmly into contact, resulting not only in a wider rim in close contact (larger seal L_r'), but also in a higher normal (compressive) force acting on it, which likely reduces h in the seal. Both factors improve the seal, thereby further increasing viscous flow resistance and hence the pressure difference. Once a threshold pressure difference has been reached, this positive feedback cycle results in a self-sealing process and hence strong increase of adhesion. It should be noted that in the adhesive regime, pull-off stresses logarithmically increased with retraction velocity (Figure 2a,b). This may be explained by the stretching of the microstructures, which leads to relatively smaller effective velocities u_{eff}/u for faster pull-offs.

The critical role of normal, compressive forces on the rim is also suggested by the better performance of microstructures with larger cup angles (15° vs 10° and 5°). Because of higher normal forces, the thickness h of the fluid film under the rim may be smaller for larger angles; this may explain why larger cup angles led to lower transition velocities and higher

adhesion. Our previous findings show that the underwater adhesion does not increase further for microstructures with even larger cup angles;[38] this is likely due to the larger amount of elastic energy stored during preload. A more complete theoretical model is currently under development.
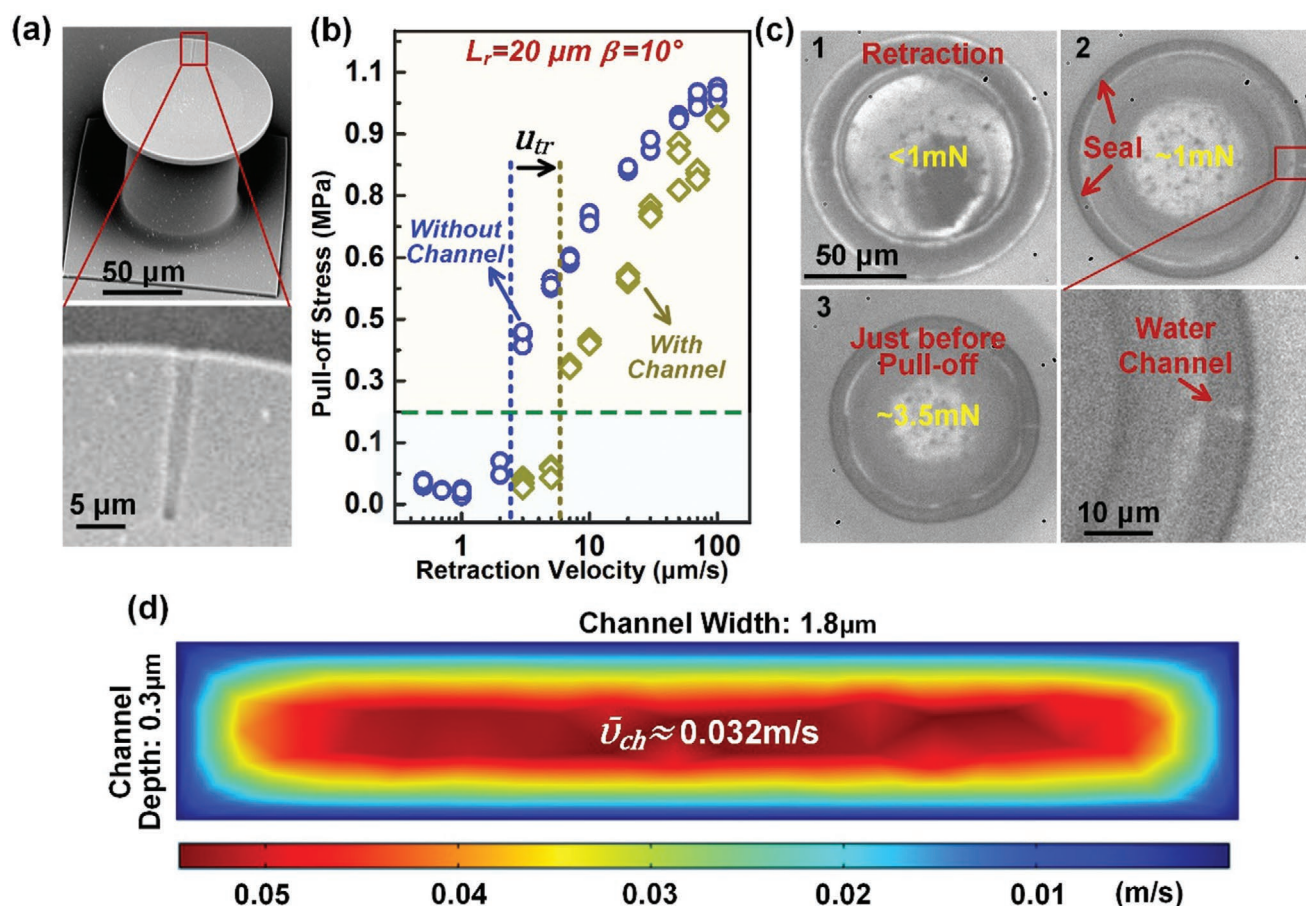
To further investigate the transition from low to high adhesion and to modulate the velocity triggering it, a 1.8 µm-wide and 0.3 µm-deep channel was radially added to the cupped microstructure design with $L_r = 20\ \mu m$ and $\beta = 10°$ (CM20/10°, **Figure 3**a). The channel allowed well-defined water flow at the interface during retraction. In the presence of the channel, the adhesion switched from low to high adhesion between 5 and 7 µm s⁻¹, which is twice the retraction velocity of the structure without the channel (Figure 3b). For each retraction velocity, pull-off stresses were lower for the microstructure with the channel compared to the channel-free structures, but similarly increased with higher velocities. Assuming that the transition from low to high adhesion takes place at a pressure difference of 100 kPa (Figure 2), we calculated the transition velocity of the cupped microstructure with and without channel. First, the average flow rate through the channel with a cross section of 0.54 µm² was numerically calculated using COMSOL Multiphysics 4.2a (Figure 3d). Figure 3d shows the velocity profile for the cross section of the channel and an average velocity of $\overline{v}_{ch} = 0.032\ m\ s^{-1}$. This results in a rate of water flow through the channel of $\dot{V}_{ch} = 17\,280\ \mu m^3\ s^{-1}$. We assume that the expansion of the cavity with channel is $\dot{V}_{cav,ch} \approx \dot{V}_{in} + \dot{V}_{ch}$, where $\dot{V}_{in}$ is, as before, the water penetration without the channel. The minimum velocity required to reach the transition from low to high adhesion at a pressure difference of 100 kPa is $u_{tr} = \frac{\dot{V}_{in}}{\pi R^2}$ for the channel-free cup (CM20/10°) and $u_{tr,ch} = \frac{\dot{V}_{cav,ch}}{\pi R^2}$ for the cup with channel. Therefore, the transition velocity for the cup with channel can be estimated as

$$u_{tr,ch} = u_{tr} + \frac{\dot{V}_{ch}}{\pi R^2} \quad (5)$$

From $u_{tr} = 2.5\ \mu m\ s^{-1}$ (see Figure 3b), $\dot{V}_{ch} = 17\,280\ \mu m^3\ s^{-1}$, and $R = 40\ \mu m$, the transition velocity is $u_{tr,ch} = 5.9\ \mu m\ s^{-1}$. This calculated value is in good agreement with the experimentally obtained values between 5 and 7 µm s⁻¹ for the transition velocity with channel. Further tests with cupped microstructures containing a larger number of microchannels, or microchannels with varying depths confirmed that the total water flow rate through the channels determines the transition velocity according to Equation (5), with more and deeper channels shifting the transition to higher velocities (Figure S1, Supporting Information).

To demonstrate the switchability of cupped microstructures in a pick-and-place process, cupped microstructures (CM10/10°) were fabricated in a square lattice of 25 mm² with 256 cups at a center-to-center distance of 300 µm (**Figure 4**a). The successful underwater handling of a 30 g weight (brass block with a smooth glass surface for adhesive contact) is demonstrated in Figure 4b,c and Video S1, Supporting Information. First, the microarray was brought in contact with the submerged brass block under a compressive preload of 300 mN. Second, the

Figure 3. Cupped microstructure with a defined flow channel. a) Scanning electron micrograph of the cupped microstructure with a channel along the rim. b) Comparison of the pull-off adhesion force between the cups with and without a channel. c) Recorded contact images in the presence of a channel. d) Cross section of the channel showing the numerically determined flow profile. The average velocity was $\overline{v}_{ch}$ was 0.032 m s^{-1} for a pressure difference of 100 kPa.

block was lifted using a high retraction velocity of 100 μm s^{-1} and held for 50 s. The tensile load was 260 mN in accordance with the weight of the submerged block. After returning the brass block to the starting position, it was released at a much lower retraction velocity of 1 μm s^{-1}. The adhesion force was 60 mN and, therefore, below the weight of the brass block. This experiment successfully demonstrates that the adhesion force can be switched by varying the retraction velocity. The effect, therefore, exhibits high potential for underwater handling of solid objects.

3. Conclusions

In summary, we presented a study on the switchable underwater adhesion of deformable cupped microstructures and their potential for micromanipulation of objects in wet or submerged conditions. Underwater adhesion was tested for different cup designs and for various retraction velocities. The following conclusions can be drawn:

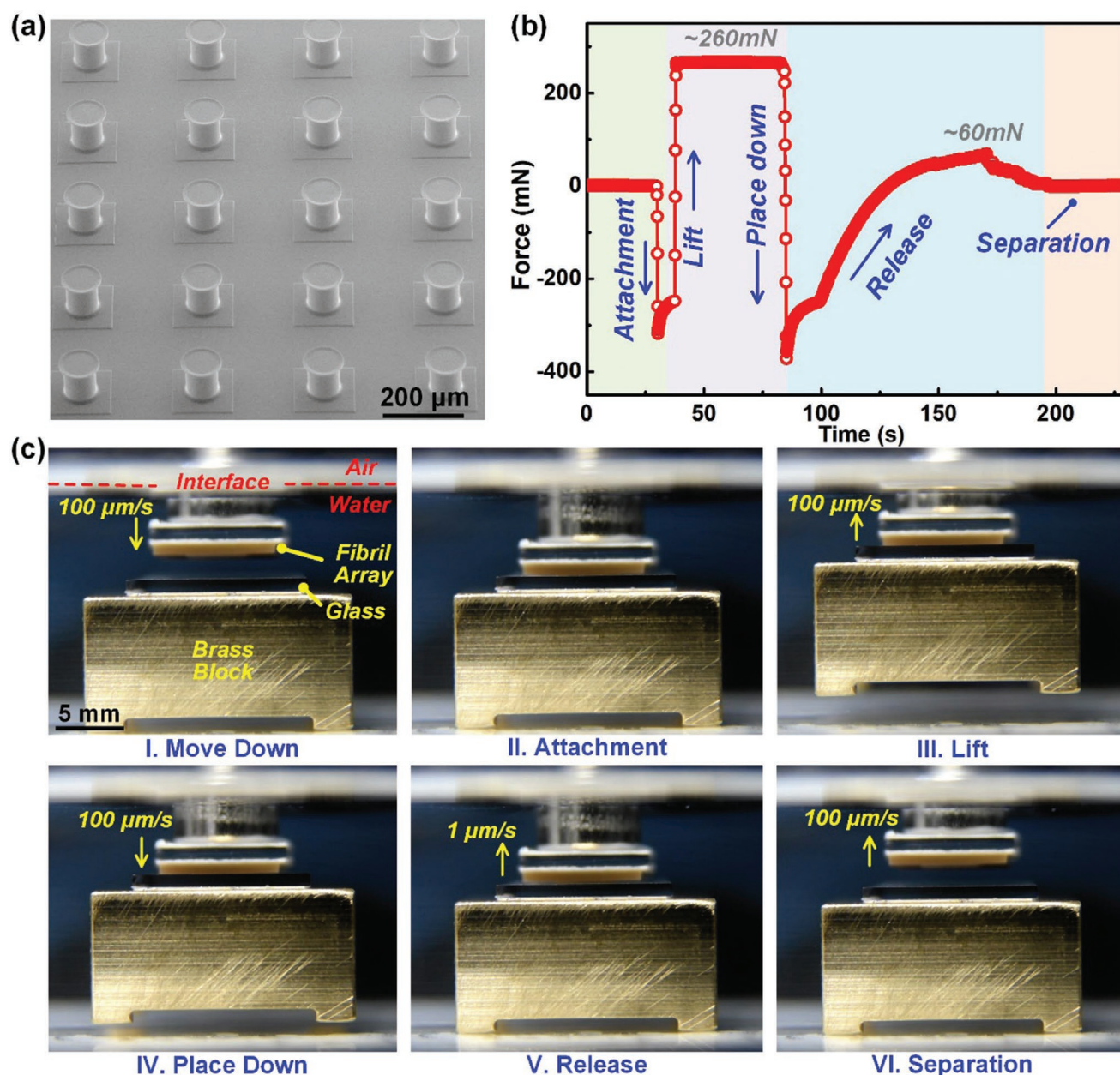1. Cupped microstructures can be switched from a low (<0.2 MPa) to a high (≈1 MPa) adhesion regime by adjusting

the retraction velocity, for the microstructures investigated from 0.5 to 20 μm s^{-1}.

2. The transition velocity depends on the cup design, such as the projected width of the rim and the cup angle. Wider rims and larger cup angles decrease the transition velocity.

3. The switchability of adhesion can be explained by the self-sealing property of cupped microstructures, whereby faster and stronger pulls lead to an improvement of the seal, further increasing adhesion.

4. Experimental Section

Fabrication of Deformable Cupped Microstructures: Cupped microstructures were fabricated as previously described by Yue et al.[38] Briefly, the designed microstructures were printed using two-photon lithography system (Photonic Professional GT, Nanoscribe, Eggenstein-Leopoldshafen, Germany).[39] Then, these structures were replicated into PU (NEUKADUR A75, Altropol GmbH, Stockelsdorf, Germany) with a Young's modulus of about 15 MPa. For the replication, molds made from polydimethylsiloxane (PDMS, SYLGARD 184, Dow Corning, Midland, USA) were used. The PU prepolymer was mixed by 1.2 parts of base and one part of cross-linker and cast onto the PDMS template. Curing of PU took place in an oven at 65 °C for at least 12 h. Upon demolding, the cupped microstructures were tested without further treatments.

**ADVANCED
SCIENCE NEWS**

www.advancedsciencenews.com

**ADVANCED
MATERIALS
INTERFACES**

www.advmatinterfaces.de

Figure 4. Demonstration of underwater pick-and-place handling using deformable cupped microstructures. a) Scanning electron micrograph of the 5×5 mm^2 array of cupped microstructures CM10/10°. b) The force versus time curve and c) the corresponding images of one entire cycle where a brass block was picked up and released under water.

Adhesion Measurements: All the tests were performed using a custom-made apparatus. A 2 mm long glass cylinder with a diameter of 2 mm was used as a nominally flat substrate. Two goniometers were used to properly align the microstructures to the substrate. A load cell (KD45-2N, ME-Messsysteme, Hennigsdorf, Germany) was utilized to record forces with a resolution of about 0.4 mN. The displacement was realized by a linear actuator (Q-545.240, PI, Karlsruhe, Germany). Data were recorded using a LabVIEW script. In addition, contact area images of the microstructures with the substrate were observed through the transparent glass cylinder using a tubular optic and monochromatic coaxial illumination (UltraZoom, Navitar, Inc., New York, NY, USA) with a wavelength of 436 nm. Videos were recorded with a camera (DMK 33UX252, Imaging Source, Bremen, Germany).

Cupped microstructures were immersed in a 50 µL droplet of distilled water for all underwater adhesion tests. The glass substrate was brought in contact with the microstructures with a compressive preload of 3 mN and held for 5 s. Then, the substrate was normally retracted until the structure detached. The maximum tensile load was defined as the pull-off force. Peak normal forces were converted into stresses by dividing them with the projected area of the cup in the original undeformed state. The retraction velocities varied from 0.1 to 100 µm s^{-1}. Each test was repeated with at least three different samples. Between the tests, the glass substrate was kept immersed in the water droplet.

Pick-and-Release Demonstration: An adhesive array of 5×5 mm^2 with 256 cupped microstructures (CM10/10°) was prepared as described above. A 1 mm-thick smooth glass substrate was glued to the top

surface of a brass block with edge lengths of 20, 20, and 10 mm, and a weight of about 30 g (in air). The brass block was placed at the bottom of a water basin, whereas the adhesive pad was fixed to the load cell (KD40S-5N, ME-Messsysteme, Germany) and a linear stage (M-404.8PD, PI, Karlsruhe, Germany). Then the adhesive array was brought in contact with the glass surface with a preload of about 300 mN, and a rate of 100 µm s^{-1}; the contact was held for 8 s. The retraction velocity was either 100 µm s^{-1} (pick and lift) or 1 µm s^{-1} (release). Upon lifting, the brass block was held (underwater) for 50 s. A side view of the process was recorded using a digital camera (Nikon D7200, Nikon Corporation, Japan).

Supporting Information

Supporting Information is available from the Wiley Online Library or from the author.

Conflict of Interest

The authors declare no conflict of interest.

[1] Y. Wang, X. Yang, Y. Chen, D. K. Wainwright, C. P. Kenaley, Z. Gong, Z. Liu, H. Liu, J. Guan, T. Wang, J. C. Weaver, R. J. Wood, L. Wen, *Sci. Rob.* **2017**, *2*, eaan8072.

[2] S. Kurumaya, B. T. Phillips, K. P. Becker, M. H. Rosen, D. F. Gruber, K. C. Galloway, K. Suzumori, R. J. Wood, *Soft Rob.* **2018**, *5*, 399.

[3] Y. F. Ma, S. H. Ma, Y. Wu, X. W. Pei, S. N. Gorb, Z. K. Wang, W. M. Liu, F. Zhou, *Adv. Mater.* **2018**, *30*, 1801595.

[4] Y. H. Zhao, Y. Wu, L. Wang, M. M. Zhang, X. Chen, M. J. Liu, J. Fan, J. Q. Liu, F. Zhou, Z. K. Wang, *Nat. Commun.* **2017**, *8*, 2218.

[5] J. J. Green, J. H. Elisseeff, *Nature* **2016**, *540*, 386.

[6] L. Li, W. Smitthipong, H. Zeng, *Polym. Chem.* **2015**, *6*, 353.

[7] S. Y. Yang, E. D. O'Cearbhaill, G. C. Sisk, K. M. Park, W. K. Cho, M. Villiger, B. E. Bouma, B. Pomahac, J. M. Karp, *Nat. Commun.* **2013**, *4*, 1702.

[8] L. Han, L. Yan, K. Wang, L. Fang, H. Zhang, Y. Tang, Y. Ding, L.-T. Weng, J. Xu, J. Weng, Y. Liu, F. Ren, X. Lu, *NPG Asia Mater.* **2017**, *9*, e372.

[9] K. Autumn, M. Sitti, Y. A. Liang, A. M. Peattie, W. R. Hansen, S. Sponberg, T. W. Kenny, R. Fearing, J. N. Israelachvili, R. J. Full, *Proc. Natl. Acad. Sci. USA* **2002**, *99*, 12252.

[10] R. Spolenak, S. Gorb, H. Gao, E. Arzt, *Proc. R. Soc. London, Ser. A* **2005**, *461*, 305.

[11] J.-H. Dirks, W. Federle, *J. R. Soc., Interface* **2011**, *8*, 952.

[12] J.-H. Dirks, W. Federle, *Soft Matter* **2011**, *7*, 11047.

[13] A. H. Hofman, I. A. van Hees, J. Yang, M. Kamperman, *Adv. Mater.* **2018**, *30*, 1704640.

[14] N. Cadirov, J. A. Booth, K. L. Turner, J. N. Israelachvili, *ACS Appl. Mater. Interfaces* **2017**, *9*, 14497.

[15] J. N. Israelachvili, *Intermolecular and Surface Forces: Third Edition*, Academic Press, San Diego, CA **2011**.

[16] H.-J. Butt, W. J. P. Barnes, A. del Campo, M. Kappl, F. Schönfeld, *Soft Matter* **2010**, *6*, 5930.

[17] A. Y. Stark, I. Badge, N. A. Wucinich, T. W. Sullivan, P. H. Niewiarowski, A. Dhinojwala, *Proc. Natl. Acad. Sci. USA* **2013**, *110*, 6340.

[18] F. Meng, Q. Liu, X. Wang, D. Tan, L. Xue, W. J. P. Barnes, *Philos. Trans. R. Soc., A* **2019**, *377*, 20190131.

[19] P. Rao, T. L. Sun, L. Chen, R. Takahashi, G. Shinohara, H. Guo, D. R. King, T. Kurokawa, J. P. Gong, *Adv. Mater.* **2018**, *30*, 18018844.

[20] R. Hensel, K. Moh, E. Arzt, *Adv. Funct. Mater.* **2018**, *28*, 1800865.

[21] V. Tinnemann, E. Arzt, R. Hensel, *J. Mech. Phys. Solids* **2019**, *123*, 20.

[22] A. B. Croll, N. Hosseini, M. D. Bartlett, *Adv. Mater. Technol.* **2019**, *4*, 1900193.

[23] H. E. Jeong, J.-K. Lee, H. N. Kim, S. H. Moon, K. Y. Suh, *Proc. Natl. Acad. Sci. USA* **2009**, *106*, 5639.

[24] B. Soltannia, D. Sameoto, *ACS Appl. Mater. Interfaces* **2014**, *6*, 21995.

[25] M. Varenberg, S. Gorb, *J. R. Soc., Interface* **2008**, *5*, 383.

[26] R. Hensel, R. Helbig, S. Aland, H. G. Braun, A. Voigt, C. Neinhuis, C. Werner, *Langmuir* **2013**, *29*, 1100.

[27] R. Hensel, A. Finn, R. Helbig, S. Killge, H.-G. Braun, C. Werner, *Langmuir* **2014**, *30*, 15162.

[28] R. Hensel, R. Helbig, S. Aland, A. Voigt, C. Neinhuis, C. Werner, *NPG Asia Mater.* **2013**, *5*, e37.

[29] B.-E. Pinchasik, J. Steinkühler, P. Wuytens, A. G. Skirtach, P. Fratzl, H. Möhwald, *Langmuir* **2015**, *31*, 13734.

[30] N. Hosoda, S. N. Gorb, *Proc. R. Soc. London, Ser. B* **2012**, *279*, 4236.

[31] S. Baik, D. W. Kim, Y. Park, T.-J. Lee, S. Ho Bhang, C. Pang, *Nature* **2017**, *546*, 396.

[32] D. K. Wainwright, T. Kleinteich, A. Kleinteich, S. N. Gorb, A. P. Summers, *Biol. Lett.* **2013**, *9*, 20130234.

[33] J. A. Sandoval, S. Jadhav, H. Quan, D. D. Deheyn, M. T. Tolley, *Bioinspiration Biomimetics* **2019**, *14*, 066016.

[34] V. Kang, R. Johnston, T. van de Kamp, T. Faragó, W. Federle, *BMC Zool.* **2019**, *4*, 10.

[35] S. Baik, H. J. Lee, D. W. Kim, H. Min, C. Pang, *ACS Appl. Mater. Interfaces* **2019**, *11*, 25674.

[36] H. Lee, D. S. Um, Y. Lee, S. Lim, H. Jun Kim, H. Ko, *Adv. Mater.* **2016**, *28*, 7457.

[37] S. Baik, J. Kim, H. J. Lee, T. H. Lee, C. Pang, *Adv. Sci.* **2018**, *5*, 1800100.

[38] Y. Wang, V. Kang, E. Arzt, W. Federle, R. Hensel, *ACS Appl. Mater. Interfaces* **2019**, *11*, 26483.

[39] J. Purtov, A. Verch, P. Rogin, R. Hensel, *Microelectron. Eng.* **2018**, *194*, 45.